Asian Journal of Pharmaceutical Sciences 17 (2022) 571–582

Available online at www.sciencedirect.com

ScienceDirect

journal homepage: www.elsevier.com/locate/AJPS

Original Research Paper

Nucleobase-crosslinked poly(2-oxazoline) nanoparticles as paclitaxel carriers with enhanced stability and ultra-high drug loading capacity for breast cancer therapy

Si Dong[a,b], *Sheng Ma*[b,d], *Hongyu Chen*[b,c], *Zhaohui Tang*[b,c,d], *Wantong Song*[b,d,*], *Mingxiao Deng*[a,*]

[a] *College of Chemistry, Northeast Normal University, Changchun 130024, China*
[b] *Key Laboratory of Polymer Ecomaterials, Changchun Institute of Applied Chemistry, Chinese Academy of Sciences, Changchun 130022, China*
[c] *University of Science and Technology of China, Hefei 230026, China*
[d] *Jilin Biomedical Polymers Engineering Laboratory, Changchun 130022, China*

ARTICLE INFO

Article history:
Received 13 February 2022
Revised 12 April 2022
Accepted 27 April 2022
Available online 31 May 2022

Keywords:
Poly(2-oxaozoline)
Nanoparticles
Paclitaxel
Nucleobase-crosslinked
Murine breast cancer

ABSTRACT

Poly(2-oxazoline) (POx) has been regarded as a potential candidate for drug delivery carrier to meet the challenges of nanomedicine clinical translation, due to its excellent biocompatibility and self-assembly properties. The drug loading capacity and stability of amphiphilic POxs as drug nanocarriers, however, tend to be insufficient. Herein, we report a strategy to prepare nucleobase-crosslinked POx nanoparticles (NPs) with enhanced stability and ultra-high paclitaxel (PTX) loading capacity for breast cancer therapy. An amphiphilic amine-functionalized POx (PMBEOx-NH_2) was firstly prepared through a click reaction between cysteamines and vinyl groups in poly(2-methyl-2-oxazoline)-block-poly (2–butyl–2-oxazoline-*co*-2-butenyl-2-oxazoline) (PMBEOx). Complementary nucleobase-pairs adenine (A) and uracil (U) were subsequently conjugated to PMBEOx-NH_2 to give functional POxs (POxA and POxU), respectively. Due to the nucleobase interactions formed between A and U, NPs formed by POxA and POxU at a molar ratio of 1:1 displayed ultrahigh PTX loading capacity (38.2%, PTX/POxA@U), excellent stability, and reduced particle size compared to the uncross-linked PTX-loaded NPs (PTX/PMBEOx). Besides the prolonged blood circulation and enhanced tumor accumulation, the smaller PTX/POxA@U NPs also have better tumor penetration ability compared with PTX/PMBEOx, thus leading to a higher tumor suppression rate in two murine breast cancer models (E0711 and 4T1). These results proved that the therapeutic effect of chemotherapeutic drugs could be improved remarkably through a reasonable optimization of nanocarriers.

* Corresponding authors.
E-mail addresses: wtsong@ciac.ac.cn (W.T. Song), dengmx330@nenu.edu.cn (M.X. Deng).
Peer review under responsibility of Shenyang Pharmaceutical University.

https://doi.org/10.1016/j.ajps.2022.04.006

1. Introduction

Polymeric therapeutics which are made up of polymer and chemotherapeutic drugs have recently emerged as a promising anticancer drug candidate, as they can potentially provide higher therapeutic efficiency and lower toxicity compared to conventional chemotherapeutics [1–5]. As so far, several polymeric therapeutics have been approved for clinical cancer therapy, such as PM-Genexol [6], Onivyde [7], and more are undergoing preclinical or clinical studies [8]. The blood vessels of tumor are generally characterized through abnormalities, such as a high proportion of aberrant basement membrane formation, pericyte deficiency and proliferating endothelial cells, causing an improved vascular permeability [9]. Thus, polymeric therapeutics are inclined to accumulate in tumor tissues in comparison to the normal tissues, defined as enhanced permeability and retention (EPR) effect [10]. Generally, polymer can assemble to form NPs ranging from 20 to 200 nm in physiological solution. Thus, there is a general agreement that polymeric therapeutic NPs can extravasate from tumor blood vessels and accumulate inside the interstitial space through EPR effect [11,12]. Although EPR effect has been widely demonstrated in many tumor models, it is still controversial as the uncertainty arises in each tumor model. In a recent report, Wilhelm et al. summarized the prior manuscripts on "nanoparticle delivery" to determine the current delivery efficiency to solid tumors. In their study, the data was tabulated and standardized to calculate the delivery efficiency of drug-loaded nanoparticles after reviewing more than 100 studies. By comparing the quantification of drug-loaded nanoparticles in blood and solid tumors, they found that only 0.7% of the injected dose of the nanoparticles could pass through physical and biological barriers (for example, diffusion, flow and shear forces, aggregation, protein adsorption, phagocytic sequestration and renal clearance) and reach the tumor by EPR effect [13]. Such low delivery efficiency may be responsible for the poor clinical transformation of nanomedicines.

The chemical and physical properties of NPs, particularly stability, dictate their ability to accomplish the therapeutic efficacy. Obviously, high stability in blood is the prerequisite for drug-loaded NPs because once drug-loaded NPs lose their integrity in the blood, they will immediately release the drugs into the blood and fail their therapeutic mission, let alone such functions as tumor accumulating via the EPR effect. Some studies have proved this view. For example, Sun et al. demonstrated that the shear and the blood-borne proteins induced 80% of NPs constructed by PEG-PCL and PEG-PDLLA to dissociate into unimers and be cleared by Kupffer cells once intravenously injected, resulting in low tumor accumulation [14]. Chen et al. reported that a part of NPs would lose their cohesion in serum mimicking conditions and even transform their structures and release their payloads immediately in circulation [15]. Thus, stability is a key factor to determine the *in vivo* performance of NPs. Various innovative strategies were established for improving the stability of non-covalent drug-loaded nanocarriers. For example, core cross-linking strategies were constantly adopted for enhancing the stability of drug-loaded NPs. Zhai et al. designed a kind of core cross-linked NPs for chemotherapeutics delivey by visible light-induced metathesis and regeneration of the diselenide bonds in di-(4,1-hydroxybenzylene) diselenide-*g*-poly(ethylene oxide)-*b*-poly methacrylic acid. Compared with non-crosslinked NPs, these core cross-linked NPs were more stable in physiological conditions and exhibited longer blood circulation, resulting in more tumor accumulation and longer tumor retention [16]. Zhou et al. developed a cross-linked micellar drug delivery system basis on N-(2-hydroxypropyl) methacrylamide (HPMA) copolymers. The hydrazone linkages in the side chains of HPMA ensured micelle stability in the blood and enhanced tumor accumulation [17]. However, these methods using the metathesis or regeneration of the unstable bonds cross-linking are complex, it is still necessary to find a simple cross-linking approach for improving NPs stability.

POxs have been investigated as biomaterials for decades resulting from their excellent hemo- and cyto-compatibility [18]. Hydrophilic poly(2-methyl-2-oxazoline) (PMeOx) and poly(2-ethyl-2-oxazoline) (PEtOx) are of particular interest since they present stealth [19,20] and protein repellent effects [21]. They also have the same rapid renal clearance as the poly(ethylene glycol) (PEG) [22], and are regarded as promising alternatives for replacement of PEG for protecting NPs from protein adsorption and blood clearance [23]. As a result, POx has been widely reported as a drug delivery platform. Han et al. have reported that amphiphilic POx NPs could act as a promising delivery platform with high drug loading capability for multidrug cancer chemotherapy [24]. Kabanov et al. demonstrated that POx NPs exhibited a relatively high drug loading capacity for drugs such as paclitaxel, docetaxel and etoposide due to the short amphiphilic side chain with a flexible polar hydrophobic micelle core [25]. However, the short side chain in hydrophobic segments also lead to some negative results on POx NPs. For example, POx NPs cannot provide a stable hydrophobic core resulting in the failure of encapsulation for some hydrophobic drugs such as imiquimod, wortmannin and SN-38 [26]. Besides, unstable hydrophobic core cannot prolong the circulation time of drug-loaded NPs *in vivo*. He et al. reported that the pharmacokinetic half-life of PTX-loaded poly(2-methyl-2-oxazoline-block-2–butyl–2-oxazoline-block-2-methyl-2-oxazoline) (P(MeOx-*b*-BuOx-*b*-MeOx)) NPs in tumor-free nude mice is only 2.8 h, which showed little improvement of Taxol (2.6 h) [27]. The reason for the phenomenon may be the hydrophobic segment of P(MeOx-*b*-BuOx-*b*-MeOx) is composed of hydrophobic poly(2–butyl–2-oxazoline) which may not provide a sufficiently hydrophobic and stable micellar core. Therefore, rational design of core cross-linked POx may be conducive to improving the blood circulation stability, prolonging the blood circulation time, and enhancing the tumor accumulation.

Herein, we prepared a novel core cross-linked amphiphilic POx complex for PTX loading (Scheme 1). Nucleobase pairs of adenine (A) and uracil (U) were chosen as the nucleobase interactions cross-linking sites in the hydrophobic core as they can easily form complementary multiple hydrogen bond interactions in an aqueous solution. The nucleobase cross-linked cores of POx NPs have numerous advantages, such as increased stability, reduced particle size, prolonged

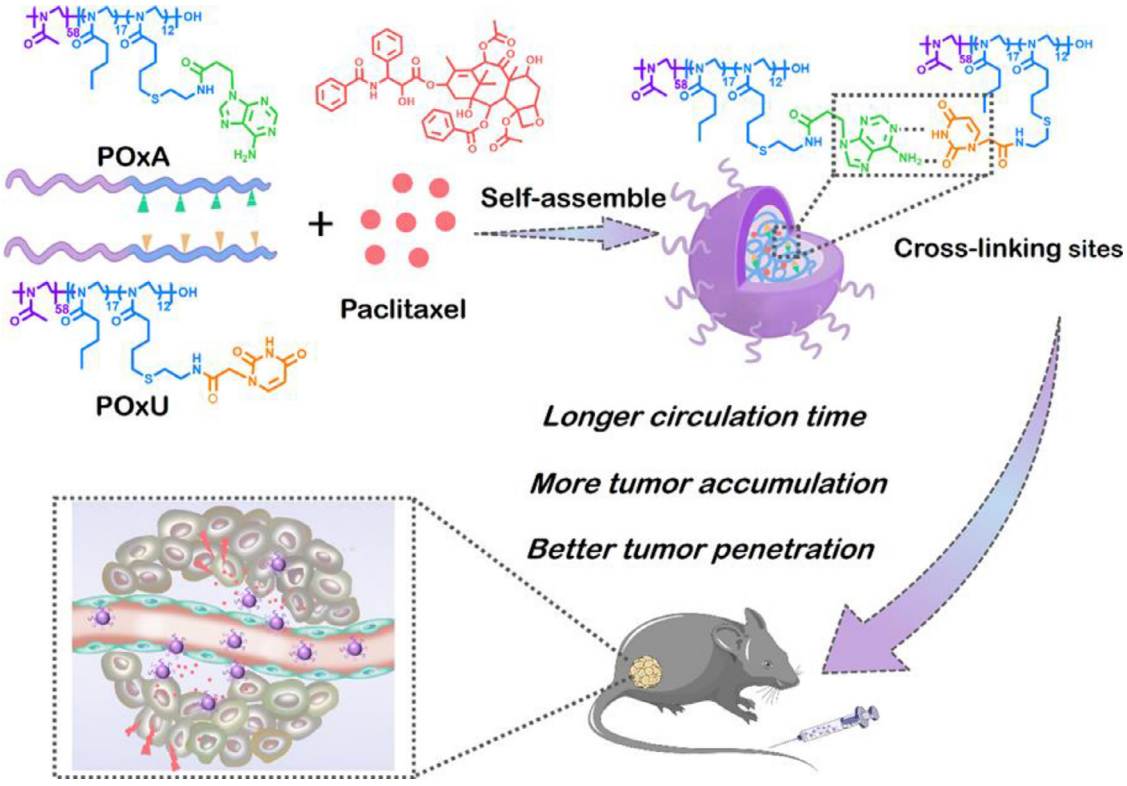

Scheme 1 – Diagrammatic illustration of preparation of the nucleobase-crosslinked PTX-loaded NPs and the NPs enter tumor tissue to kill tumor cells.

blood circulation time, and promoted tumor accumulation as well. More importantly, due to the smaller size of core cross-linked NPs, the tumor tissue permeability of NPs was much better than that of non-cross linked POx NPs, which resulted in stronger tumor suppression ability in two murine breast cancer models. Given that PTX is widely used in the clinical treatment of breast cancer, this PTX-loaded core cross-linked POx NPs holds great clinical translation value and may benefit a broad range of patients.

2. Materials and methods

2.1. *Materials*

Ethyl acrylate, bromoacetic acid, adenine, uracil, N,N'-diisopropylcarbodiimide (DIC), and 4-dimethylaminopyridine (DMAP) were purchased from Energy Chemical Co., LTD. (Beijing, China). 3-(4,5-Dimethyl-thiazol-2-yl)−2,5-diphenyl tetrazolium bromide (MTT), and 4′,6-diamidino-2-phenylindole dihydrochloride (DAPI) were purchased from Sigma-Aldrich Co. LTD (Shanghai, China). 1,1-Dioctadecyl-L-3,3,3,3-tetramethylindodicarbocyanine perchlorate (DiD), Nile Red and PTX were purchased from Beijing J&K Co., LTD. (Beijing, China). Other organic solvents and chemical reagents were purchased from Sinopharm Chemical Reagent Co., LTD.

2.2. *Characterization*

Bruker AV-300 NMR spectrometer was applied for characterizing ^{1}H NMR spectra. Gel permeation chromatography (GPC) measurements were conducted on a Waters GPC system. The eluant was DMF (containing 0.01 M LiBr) with a flow rate of 1.0 ml/min and monodisperse polystyrene as standard samples. The amount of PTX of drug release experiment and biodistribution experiment were measured by high performance liquid chromatography (HPLC) which was conducted via a PerkinElmer Flexar system. Dynamic light scattering (DLS) which was performed on Malvern Zetasizer instrument (Nano-ZS90) was used to characterize the self-assemble and the sizes of NPs. A JEOL JEM-1011 transmission electron microscopy (TEM, Tokyo, Japan) was used to obtain the morphology images of the self-assemble NPs. Optical microscope (Nikon Eclipse Ti, Optical Apparatus Co., Ardmore, PA, USA) was used to observe histological alterations. The immunofluorescence slides were imaged on a Carl Zeiss LSM 700 confocal laser scanning microscope (CLSM).

2.3. *Synthesis of 3-(9-adeninyl)-propionic acid (A-COOH)*

As shown in Scheme S1, the preparation of A-COOH was based on the previous literature [28]. Firstly, adenine (8.0 g, 59.2 mmol) in 100 ml ethanol was added with sodium (96.0 mg, 2.6 mmol) under stirring at room temperature (RT). Once the sodium disappeared, ethyl acrylate was added into solution

and followed by heating reflux for 6 h. After the mixture was cooled down to RT, the ethanol was removed by rotary evaporation. Then purify the residue adopting cold ethanol and dry them in vacuum for obtaining 3-(6-aminopurine-9-yl)-propionic acid ethyl ester (A-COOEt 12.1 g, 86.1%). (Fig. S1)

A-COOEt (4 g, 17 mmol) was dissolved in HCl solution and refluxed for 3 h. After adding NaOH, the pH value of the solution was adjusted to 3. the residue was washed by cold water to obtain the final A-COOH (3.2 g, 91.0%). (Fig. S2)

2.4. Synthesis of 1-(carboxymethyl) uracil (U-COOH)

As shown in Scheme S1, U-COOH was prepared based on the previous literature [29]. Firstly, uracil (10.0 g, 89.2 mmol) and KOH (22.0 g, 392.8 mmol) were dissolved in 100 ml water. Then bromoacetic acid (22.0 g, 159.4 mmol) was added and stirred at 100 °C for 1 hour. After the mixture was cooled to RT, the pH value was adjusted to 2 or 3 by adding HCl solution. The precipitate was washed by water, ethanol, and ethyl acetate to obtain U-COOH (12.4 g, 81.6%). (Fig. S3)

2.5. Synthesis of adeninyl-grafted PMBEOx (POxA) and uracil-grafted PMBEOx (POxU)

The amphiphilic block copolymer cysteamine-grafted PMeOx-*b*-P(nBuOx-*co*-ButenOx (PMBEOx-NH_2) was prepared for further conjugating adenine according to our previous report [30]. The modification procedure of POxA was as follows. A-COOH (0.4 g, 2.0 mmol), DMAP (0.1 g, 0.75 mmol), and PMBEOx-NH_2 (0.7 g, 1.2 mmol amino groups) were dissolved in dry DMF (20 ml). Then DIC (0.8 g, 4.0 mmol) was added after the mixture was cooled to 0 °C. The solution was stirred at RT for 48 h. After that POxA was purified in a dialysis bag (MWCO = 3500 Da) against DMSO for 24 h and dialysis against distilled water for 48 h. POxA was finally obtained by lyophilization. Yield: 85.1%. The preparation of POxU was similar to that of POxA expect the use of U-COOH instead of A-COOH. Yield: 87.2%.

2.6. Preparation of PTX-loaded NPs

All the PTX-loaded POx NPs were prepared through thin-film method according to the literature [30]. As for PTX-loaded nucleobase cross-linked NPs (PTX/POxA@U NPs), predetermined amounts of PTX, POxA and POxU (mass ratio 1/4.6/4.4 to 5/2.6/2.4) were dissolved in ethanol at RT. Then ethanol was removed to obtain the dried film. Then DI water was added to dissolve the dried film and the blend was heated at 50 °C for 5 min. Insolubilized PTX was separated through filtration (0.22 μm pore size). PTX/POxA@U NPs were finally obtained after lyophilization. PTX/PMBEOx NPs were prepared by a similar method described above.

2.7. HPLC analysis of drugs in POx NPs

PTX loaded in POx NPs were quantified through HPLC. The mobile phase was a mixture of acetonitrile (ACN) and water in a ratio of 8:2 (v/v). The column temperature was set at 30 °C, and the flow rate was 1.0 ml/min. The detection wavelength was set at 227 nm. The sample was dissolved in the mobile phase to disintegrate the micelles and injected 20 μl into the HPLC system. The drug loading capability (DLC) and drug loading efficiency (DLE) were computed by equations below:

$$DLC\ (\%) = \frac{M_{drug}}{M_{drug} + M_{excipient}} \times\ 100\%$$

$$DLE\ (\%) = M_{drug}/M_{drug\ added} \times\ 100\%$$

Where, M_{drug} and $M_{excipient}$ were the weight of the drug and polymer separately; $M_{drug\ added}$ was the weight of the drug added in the preparation of the NPs formulation.

2.8. Solution behavior of PTX-loaded NPs

The hydrodynamic diameter and poly dispersity index (PDI) of the NPs prepared above were determined through dynamic light scattering (DLS). Briefly, all the specimens were dissolved adopting DI H_2O for yielding 1 mg/ml ultimate NPs concentration before testing. The intensity means z-averaged particle size (effective diameter) was measured by cumulate analyses. Results were the average of three independent determinations. The TEM image was used to confirm the morphology of POx NPs according to the literature report [31].

2.9. Kinetic stability of POx NPs

Nile Red was used as a probe for testing the stability of POx NPs as described in the literature [32]. Nile Red (0.5 mg), equimolar POxA (5.1 mg) and POxU (4.9 mg), or 10.0 mg PMBEOx were dissolved in ethanol (50 ml) at RT and mixed them well. The ethanol was removed to obtain the dry film. Then DI water (10 ml) was dropwise added for dissolving the dried film. The blend was heated for 5 min at 50 °C. Insolubilized Nile Red was separated through filtration.

The stabilities of Nile Red/PMBEOx and Nile Red/POxA@U NPs were studied by monitoring the fluorescence emission intensity every 12 h in 0.01 mol/l phosphate buffered saline (PBS) at 25 °C. The detection of fluorescence emission intensity was to measure the emission intensities from 570 to 720 nm at 543 nm excitation wavelength.

2.10. In vitro drug release

The PTX release from POx NPs was investigated with the membrane dialysis approach against PBS of pH 7.4 and 5.5 containing 1 wt% Tween-80 at 37 °C. 10 mg PTX/PMBEOx or PTX/POxA@U NPs were dissolved in 5 ml PBS in a dialysis bag (MW 100 k Da). Then the dialysis bag was submerged in 45 ml PBS under shaking (100 rpm) at 37 °C. 4.0 ml the solution was taken out and 4.0 ml fresh PBS was added at each scheduled time point. The released PTX after 144 h was measured by HPLC.

2.11. Cell lines and cell culture

The murine breast cancer E0771 and 4T1 cell lines were employed for the *in vitro* and *in vivo* experiments. E0771

and 4T1 cells were cultured with Roswell Park Memorial Institute (RPMI) 1640 containing 50 U/ml streptomycin, 50 U/ml penicillin, and 10% fetal bovine serum, and incubate at 37 °C in an atmosphere of 5% CO_2.

2.12. *In vitro cytotoxicity assay*

In vitro cytotoxicity of free PTX and PTX-loaded POx NPs was investigated adopting MTT assay. 4T1 or E0771 cells were seeded in 96-well plates with 8000 cells per well and incubated for 12 h before treatments. Then the culture medium was moved out and replenished by a fresh medium containing PTX (0.01–100 μmol/l). After further incubation for another 24 or 48 h, 20 μl MTT reagents were added into the plates for 4 h incubation. Then, the MTT solution was moved out and supplemented by 150 μl DMSO. The absorbances of all the wells were texted at 490 nm employing a microplate reader. The cell viability (%) was the specific value of the absorbance values of specimen wells and those of control wells.

2.13. *Animal declaration*

All animal procedures were performed following the guidelines of the Institutional Animal Care and Use Committee of Jilin University. Female Sprague Dawley (SD) rats (body weight 220 g) were purchased from Beijing Huafukang Biological Technology Co. Ltd. (Beijing, China). Female BALB/c and C57BL/6 mice (6-8 week old) were purchased from Beijing Vital River Laboratory Animal Technology Co., Ltd. (Beijing, China). For 4T1 and E0771 tumor prevention model, 2×10^6 tumor cells were injected into the fourth left flank mammary fat pad of BALB/c or C57BL/6 mice.

2.14. *Pharmacokinetics study*

SD rats were randomly divided into three groups ($n = 3$), which were intravenously injected free PTX (15 mg PTX/kg, dissolved by a blend of PBS, dehydrated ethanol, and Cremophor EL® = 8:1:1), PTX/PMBEOx (15 mg PTX/kg, dissolved in PBS) or PTX/POxA@U (15 mg PTX/kg, dissolved in PBS), respectively. At defined time points (0.5, 1, 2, 4, 8, 12 and 24 h), blood specimens (250 μl) were sampled from the orbital cavity. After the specimens were heparinized and centrifuged, 750 μl acetonitrile (ACN) was mixed with plasma and the samples were vortexed for 2 min followed by centrifugation. The supernatant was used to detect PTX concentration by HPLC. The half-life ($T_{1/2}$) of the PTX and area under the PTX concentration–time curve in plasma ($AUC_{0\text{-}t}$) were computed by adopting PKSolver [33].

2.15. *Biodistribution study*

BALB/c mice (average body weight 17 g, 6 weeks old) were inoculated in the fourth left flank mammary fat pad with 4T1 breast carcinoma cells (2×10^6). Once the tumor volume was nearly 200 mm^3, mice received free PTX, PTX/PMBEOx, or PTX/POxA@U NPs with the same PTX dose (10 mg/kg), respectively ($n = 3$). Mice were sacrificed for excising tumor tissues and main organs (kidney, spleen, liver, lung, and heart) at desired time points (4 h and 24 h). The tissues were weighed and ground into pieces and then mixed with ACN and vortexed for 30 s. The supernatant was detected through HPLC.

2.16. *Tumor penetration study*

DiD-loaded POx NPs were prepared for tumor penetration study. DiD (1.0 mg), equimolar POxA (9.7 mg), and POxU (9.3 mg) were mixed well in ethanol at RT. The ethanol was removed to for obtaining the dry film. The dried film was dissolved in DI water (10 ml) and heated for 5 min at 50 °C. Insolubilized DiD was separated through filtration. The penetration of DiD/PMBEOx and DiD/POxA@U NPs was studied in 4T1 tumor model. Once tumor volume reached 200 mm^3, DiD/PMBEOx and DiD/POxA@U NPs were intravenously injected into the tumor-bearing mice (DiD dose: 2 mg/kg), respectively ($n = 3$). Mice were sacrificed 24 h after *i.v.* injection to excise tumor tissues and conduct them on paraffin embedded tumor slices after dehydration. Immunofluorescence analysis was performed applying antibodies against CD31 (stained for blood vessels) and DAPI (stained for nuclei) according to the literature report [34] and imaged with CLSM.

2.17. *In vivo antitumor efficiency*

4T1 or E0771 breast carcinoma cells (2×10^6) were injected into the fourth left flank mammary fat pad of female mice of 6–8 weeks old. Once the tumor volume was nearly 70 mm^3, mice were randomly divided into 5 groups to receive the treatment of PBS, PTX (10 mg/kg, dissolved by the blend of PBS, dehydrated ethanol, and Cremophor EL® = 8:1:1, *i.v.*), PTX/PMBEOx (10 mg PTX /kg, *i.v.*) or PTX/POxA@U (10 mg PTX /kg, *i.v.*). The mice received treatments every other day and received four times of treatments in total. Body weights and tumor volumes (V) were registered every other day. Tumor volumes were measured by calipers and calculated as following:

$$V = a \times b^2/2$$

Where, "*a*" was the main axis; "*b*" was the minor tumor axis.

The tumor suppression rate (TSR) was computed as below:

$$TSR(\%) = (V_C - V_X)/V_C$$

Where, "Vc" was the average V of the PBS group; "Vx" was the average V of the treatment group.

Mice were sacrificed and identified as terminal points if the V was above 2000 mm^3

2.18. *Statistical analysis*

Each experiment was performed at least 3 times or had 3 or more replicate samples and expressed as average ± standard deviation (SD). To compare between two groups, student's t-detection was employed. To compare between multiple groups, one-way ANOVA was adopted.

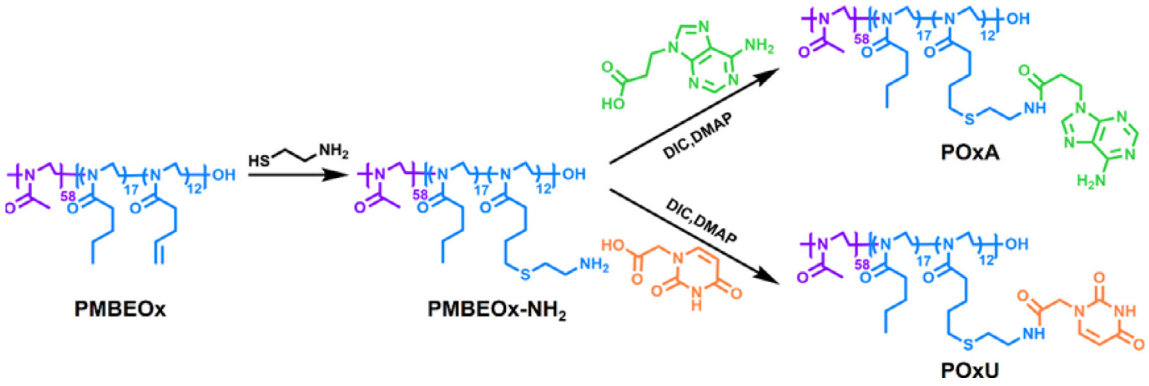

Fig. 1 – Synthesis routes of POxA and POxU.

3. Results and discussion

3.1. *Characterization of amphiphilic nucleobases grafted POx and the interaction of complementary multiple hydrogen bonds between A and U*

POxA and POxU were synthesized by grafting carboxyl-terminated nucleobases (A-COOH and U-COOH) onto amphiphilic POx. For this purpose, block copolymer bearing amino groups (PMBEOx-NH_2) and A-COOH and U-COOH were prepared (Fig. 1, Scheme S1 and Fig. S1-S3). PMBEOx was firstly synthesized as the starting polymer by living cationic ring-opening polymerization [35], and further reacted with cysteamine to obtain PMBEOx-NH_2 via radical thiol-ene addition reaction with the presence of photoinitiator I2959 under UV light (365 nm) at RT. The nucleobase-modified POxA and POxU through condensation reaction between the amino groups on PMBEOx-NH_2 and the carboxyl groups on nucleobases (A-COOH, U-COOH). As shown in Fig. 2A, the complete disappearance of the signals of the protons associated with the double bond of PMBEOx (j, $\delta = 4.78–4.85$ ppm; k, $\delta = 5.75$ ppm), and the appearance of characteristic proton signals corresponding to cysteamine (m, $\delta = 3.21$ ppm; l, $\delta = 2.89$ ppm) proved the successful synthesis of PMBEOx-NH_2. After nucleobase modification, the characteristic peaks of adenine derivatives appeared at 4.34 (o), 7.28 (p) and 7.93–8.26 (q, r, s) ppm, while those of uracil derivatives appeared at 5.53 (u), 7.52 (v), 8.30 (w) and 11.23 (x) ppm in ^{1}H NMR spectrum. Through comparison of the characteristic feature peaks intensities of PMBEOx at 3.10 ppm (h) with that of A-COOH at 7.28 ppm (p) or that of U-COOH at 5.53 ppm (u), we find out that every amine groups on PMBEOx-NH_2 were modified with corresponding nucleobases.

As shown in Fig. 2B, after grafting nucleobases, the GPC traces of POxA and POxU were exhibited a clear shift to the higher molecule weight region with short retention time, in comparison with that of PMBEOx. The number-average molecular weight (Mn) of POxA was 18.2 k Da with a poly dispersion index (PDI) of 1.46, and the Mn of POxU was slightly lower than that of POxA, 15.4 k Da with PDI of 1.36. A combination of ^{1}H NMR and GPC verified that the modification reaction proceeded completed in 48 h, yielding POxA and POxU with high grafting efficiency.

The complementary multiple hydrogen bond interactions between POxA and POxU were investigated in a blend of DMSO$_{-d6}$ and $CDCl_3$ (1:1, v/v) at 25 °C. The chemical shift of the N–H resonance in U moved downfield due to the associated A and U [36]. As shown in Fig. 2C, the amide protons in POxU switched from 10.84 ppm to 11.27 ppm in the prescience of POxA, and the peak shape was also changed from sharp peak to gradual peaks. The changes of chemical shift with the increase of temperature could be attributed to the dissociation of the complementary hydrogen bonds [37]. In our research, the formation of complementary multiple hydrogen bonds between POxA and POxU was also demonstrated by variable-temperature ^{1}H NMR spectroscopy of blending two polymers with an equivalent molar ration in DMSO$_{-d6}$/$CDCl_3$ (1:1, v/v) solution (Fig. S4). The chemical shift of the N–H in POxU shifted from 11.27 to 10.96 ppm, as the temperature was raised from 25 to 45 °C. Similarly, the resonance of NH_2 shifted from 7.59 to 7.45 ppm. All the results demonstrated the formulation of a complementary base hydrogen bond between POxA and POxU.

3.2. *Preparation and characterization of PTX-loaded POx*

The complete formulation of hydrogen bonding interactions between A and U was conducive to enhancing the stability of the POx NPs constructed by POxA and POxU (POxA@U). Thus, the molar ratio of POxA to POxU was fixed at 1:1 for assembly. [28] To evaluate the PTX loading capability of POxA@U and the PMBEOx, various mass ratios of PTX and POxA@U or PMBEOx were investigated by DLC and DLE (Table 1). As shown in Fig. 3A, the maximum DLC of PTX/PMBEOx was about 17.7 wt%. Moreover, with the increase of PTX mass ratio, the DLE of PTX/PMBEOx decreased and the DLC of PTX/PMBEOx was almost constant, which was consist with our previous study [30]. In contrast, the maximum DLC of PTX/POxA@U was elevated to 38.3 wt% as the mass ratio of PTX to POxA@U increased to 4:6. The DLC of core cross-linked NPs for PTX was much higher than that of several potentially safer formulations, such as Abraxane (less than 10 wt%) [38], Genexol-PM (17 wt%) [39] and NK105 (23 wt%) [40]. The improvement of DLC caused by the core cross-linked structure was similar to previous reports. Thomas et al. developed

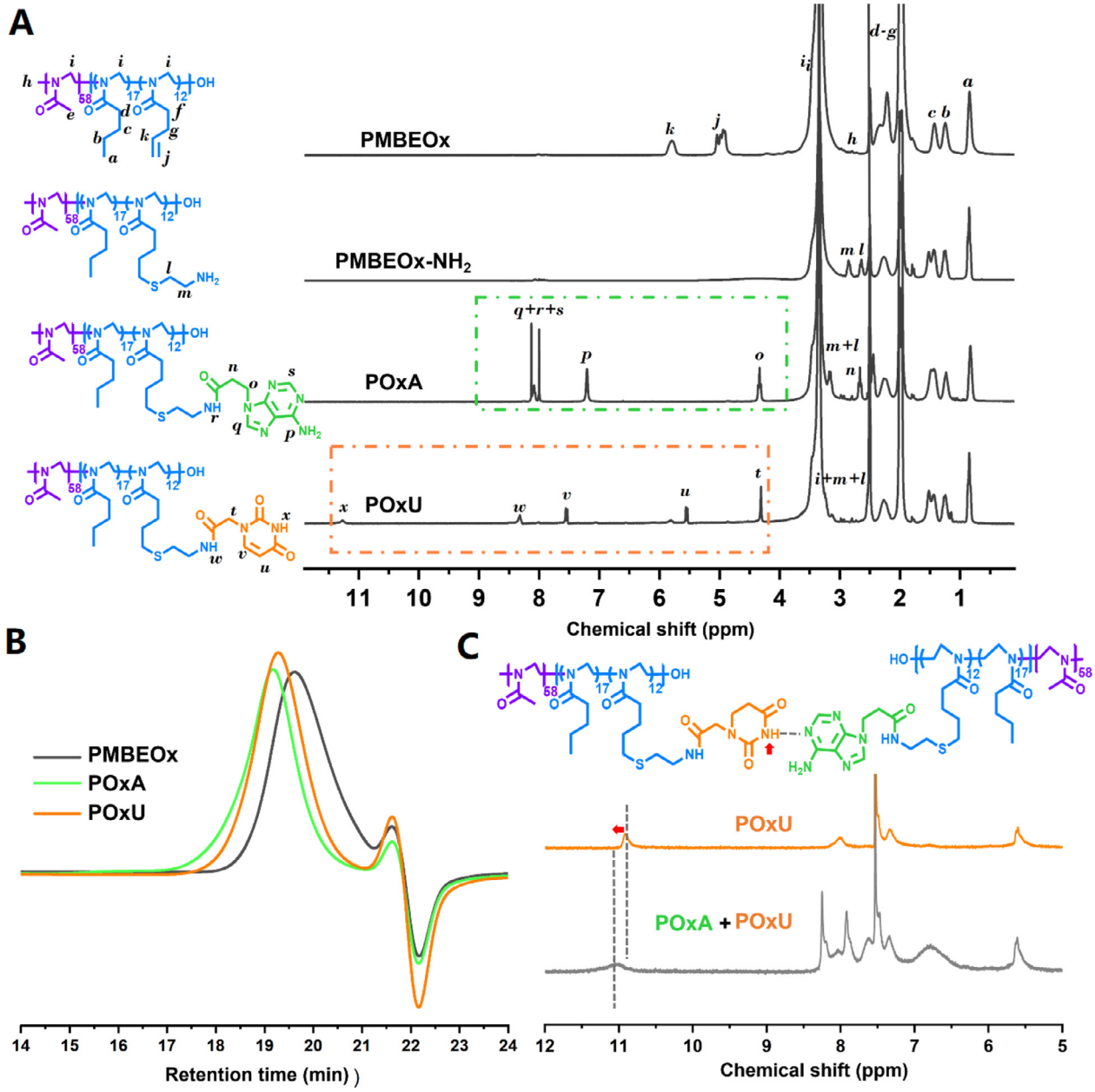

Fig. 2 – (A) ^{1}H NMR spectra of PMBEOx, PMBEOx-NH_2, POxA, and POxU in DMSO-$_{d6}$. (B) GPC curves of PMBEOx, POxA, and POxU. (C) ^{1}H NMR spectra change of the amide signal of the POxU after the addition of equivalent quality POxA in DMSO-$_{d6}$/$CDCl_3$ (1:1, v/v).

a novel core cross-linked amphiphilic copolymer based on poly(ε-caprolactone) (PCL) and monomethoxyl poly(ethylene glycol) (mPEG) for PTX encapsulating and the paclitaxel-loading efficiency of micelles was enhanced significantly upon micelle core cross-linking [41]. In our research, the DLC of both PTX/POxA and PTX/POxU NPs were less than 5 wt%, which demonstrated that the modification of adenine groups and uracil groups greatly reduced the encapsulation ability of PTX without core cross-linking structure. It was worth to point out that neither POxA@A nor POxU@U alone could be used as stable and efficient nanocarriers for encapsulating PTX. Therefore, the ultrahigh DLC was achieved from the formation of the complementary hydrogen bond interactions between POxA and POxU.

In order to reach the maximum DLC, the mass ratio of PTX to POxA@U and PTX to PMBEOx were fixed to 4:6 and 2:8 for further studies. In addition, due to the hydrogen bond interactions of the complementary nucleobases, the size of PTX/POxA@U was much smaller than PTX/PMBEOx, which was more suitable for tumor accumulation and penetration (Fig. 3B and Table 1) [42]. Both PTX/POxA@U and PTX/PMBEOx performed regular sphere morphology. (Fig. 3C)

We further evaluated the stability of POx NPs with a hydrophobic dye Nile Red in PBS (0.01 M, pH 7.4) at 25 °C as the

Table 1 – Characteristics of PTX-loaded NPs.

Mass ratio (*w*/*w*)	DLC (%)	DLE (%)	Size (nm)	PDI
PTX/PMBEOx				
1/9	9.8	98.2	101.1	0.242
2/8	17.7	88.6	115.4	0.233
3/7	17.3	57.6	116.1	0.239
4/6	16.9	42.3	115.9	0.231
5/5	17.1	34.4	115.2	0.224
PTX/POxA@U				
1/9	9.9	99.4	34.5	0.187
2/8	19.6	97.8	35.8	0.167
3/7	28.9	96.4	38.1	0.188
4/6	38.3	95.6	39.7	0.175
5/5	36.2	72.5	40.1	0.205

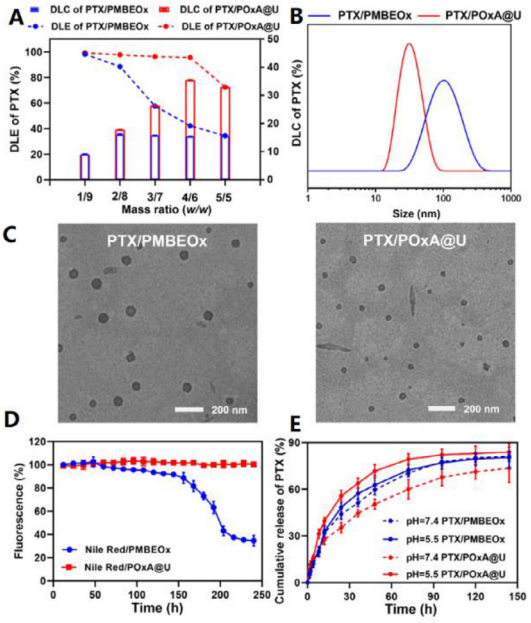

Fig. 3 – (A) Results of DLE and DLC of PMBEOx (blue) and POxA@U (red) under different mass ratios. Each data point was exhibited as an average of the three measurements. (B) Size distribution analysis of PTX/PMBEOx (blue) and PTX/POxA@U (red) after preparation. (C) TEM images of PTX/PMBEOx and PTX/POxA@U. Scale bar = 200 nm. (D) Fluorescent intensity changes of Nile Red loaded NPs over time at RT. Error bars denote the SD ($n = 3$). (E) Release study of PTX/PMBEOx (blue) and PTX/POxA@U (red) for 144 h at 37 °C in pH 7.4 or 5.5 ($n = 3$).

literature reported [32]. As shown in Fig. 3D and S5, almost no Nile Red was released from Nile Red/POxA@U in physiological conditions within 240 h post testing period. In contrast, Nile Red gradually leaked from Nile Red/PMBEOx, and less than 30% of total amount of Nile Red was left after 240 h. These results proved that the core cross-linked POx was much more stable than PMBEOx. The *in vitro* drug release profiles of PTX/POxA@U and PTX/PMBEOx were further investigated. As illustrated in Fig. 3E, the PTX release from the PTX/POxA@U was slightly slower than that from PTX/PMBEOx at pH 7.4, which may be attributed to the hydrogen bonds cross-linking induced by complementary nucleobases. The amount of PTX released PTX/PMBEOx and PTX/POxA@U was about 83% and 69% at the end 144 h, respectively. The hydrophilicity of the nucleobases was improved resulting from the tertiary amine protonation under an acidic condition, the hydrogen bonds between A and U tended to dissociate [43], causing the fast release of PTX from PTX/POxA@U under pH 5.5 PBS condition. This phenomenon could be beneficial for realizing the drug quick release rate, since the PTX/POxA@U was endocytosed into the acidic endosome of tumor cells [44]. While, the release rate of uncross-linked PTX/PMBEOx did not show any obvious changes in pH 5.5 PBS.

3.3. *In vitro cytotoxicity of PTX-loaded POx NPs*

The biocompatibility of PMBEOx, POxA, or POxU was firstly evaluated on 4T1 and E0771 tumor cell lines via MTT assays. After incubated for 24 h, no significant cytotoxicity was on 4T1 and E0771cells up to 5 mg/ml (Fig. S6A-S6B), indicating POx and modified POx all owned good biocompatibility.

The cytotoxicities of PTX-loaded POx NPs were also evaluated against 4T1 and E0771 tumor cells via MTT assay. As exhibited in Fig. 4A-4B, the IC50 value of free PTX to E0771 cells was 3.9 mmol/ml at 24 h, while for PTX-loaded NPs of PTX/PMBEOx and PTX/POxA@U were 12.8 and 8.6 mmol/ml, respectively. While, with the incubation time increasing to 48 h, cytotoxicities of PTX/PMBEOx and PTX/POxA@U were enhanced which almost matched with that of free PTX. As for 4T1 cells (Fig. 4C-4D), the IC50 value of free PTX was 1.9 mmol/ml at 24 h, while the IC50 values of PTX/PMBEOx and PTX/POxA@U were 7.6 and 11.9 mmol/ml. When the incubation time came to 48 h, IC50 values of free PTX, PTX/PMBEOx and PTX/POxA@U to 4T1 cells were 0.6, 1.3 and 1.9 mmol/ml, respectively. Alhough both PTX/PMBEOx and PTX/POxA@U exhibited slightly lower toxicity than free PTX in 4T1 and E0771 cells, they both showed similar cytotoxicity as free PTX.

3.4. *Pharmacokinetics, biodistribution and tumor penetration*

We investigated the property of the PTX-loaded POx NPs with or without cross-linked core in blood, organs, and tumors. The pharmacokinetics of free PTX, PTX/PMBEOx, and PTX/POxA@U were studied in SD rats. As illustrated in Fig. 5A, as the cross-linked core in PTX/POxA@U made the NPs more stable *in vivo*, and the circulating half-life of PTX/POxA@U was obvious longer in comparison to free PTX and PTX/PMBEOx, nearly 4.5 folds longer than that of free PTX and nearly 2 folds longer than that of PTX/PMBEOx. Free PTX was fast eliminated from blood circulation and could not be detected 12 h after injection. As Table 2 presented, the AUC_{0-t} of the PTX/POxA@U was 125.63 ± 13.60 μg/ml·h which was nearly 1.5 folds higher than that of PTX/PMBEOx (83.52 ± 12.09 μg/ml·h) and 9.23 folds higher than that of the free PTX (13.36 ± 3.47 μg/ml·h), respectively. These results demonstrated enhanced stability induced by nucleobases complementary interactions could improve the blood circulation time of POx NPs.

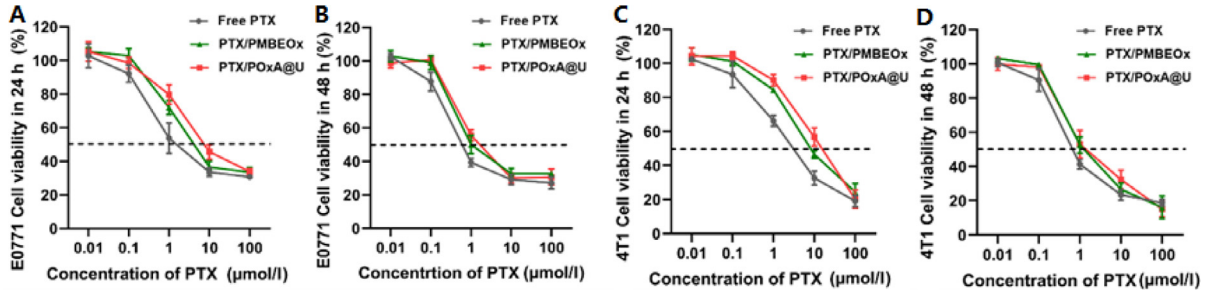

Fig. 4 – *In vitro* cytotoxicity of PMBEOx, POxA and POxU to (A-B) E0771 cells and (C-D) 4T1 cells at various PTX concentrations after incubated for 24 h or 48 h ($n = 3$).

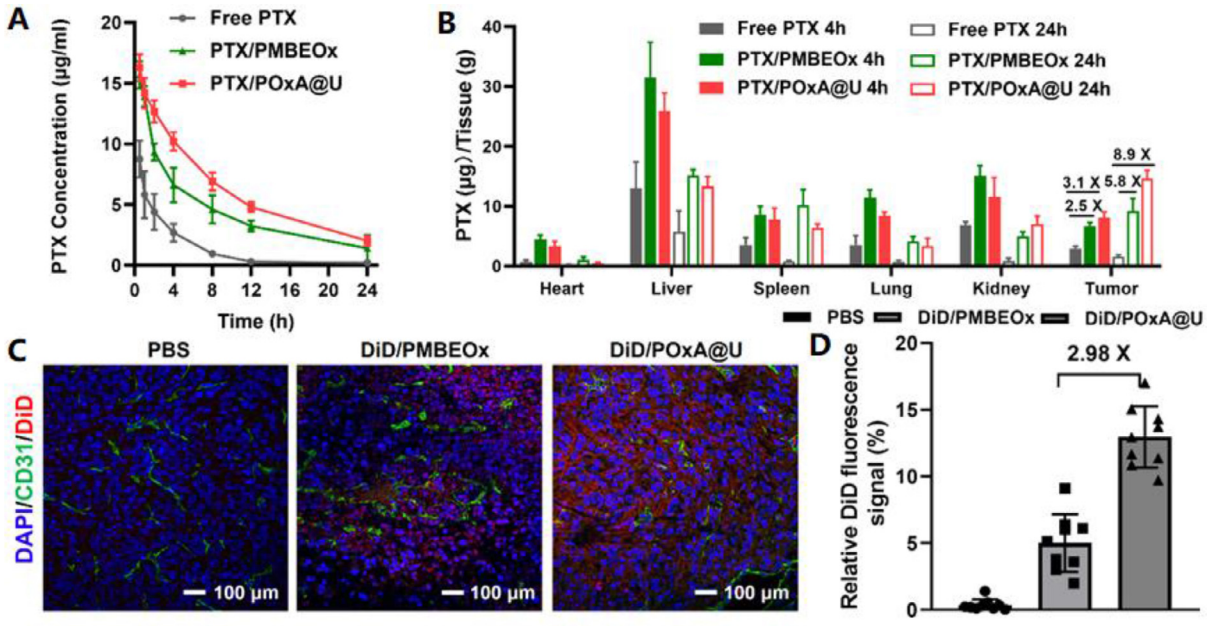

Fig. 5 – (A) Time profiles of PTX concentration in plasma after administering via tail vein of free PTX, PTX/PMBEOx and PTX/POxA@U in SD s. Each PTX formulation was equivalent PTX dose of 15 mg/kg. Data were exhibited as averages ± SD ($n = 3$). (B) Biodistribution results of free PTX, PTX/PMBEOx and PTX/POxA@U in 4T1 tumor-bearing mice. Each PTX formulation was administered at a dose of 10 mg/kg. Data were exhibited as averages ± SD ($n = 3$). (C) Confocal fluorescence images of 4T1 tumor slices at 24 h post intravenous injection. The red, blue and green signals were from the DiD, DAPI stained nuclei, and FITC fluorescence from blood vessel, respectively. (D) Quantitative analysis data of DiD fluorescence signals in tumor slices ($n = 9$).

Table 2 – Pharmacokinetic parameters for free PTX, PTX/PMBEOx and PTX/POxA@U in SD rats.

	$T_{1/2}$ [a] (h)	AUC_{0-t} [b] (μg/ml·h)
PTX	1.09 ± 0.68	13.36 ± 3.47
PTX/PMBEOx	2.68 ± 1.29	83.52 ± 12.09
PTX/POxA@U	4.98 ± 1.13	125.63 ± 13.60

[a] $T_{1/2}$: half-life of the PTX.
[b] AUC_{0-t}: area under the PTX concentration–time curve in plasma.

The biodistribution of free PTX, PTX/PMBEOx, and PTX/POxA@U was studied on 4T1 tumor-bearing mice. As Fig. 5B exhibited that after one intravenous injection, free PTX quickly diffused and cleared out from all organs. In contrast, PTX loaded in cross-linked NPs presented good distribution in tumor tissue and the tumoral concentration of PTX in PTX/POxA@U treated group was as 8.9 times as that of free PTX treated groups at 24 h, which could result from longer blood circulation time of PTX/POxA@U. Besides, because the size of PTX/POxA@U was smaller than PTX/PMBEOx, the lower liver accumulation of PTX/POxA@U could also be observed in Fig. 5B.

Next, we used the fluorescent molecule DiD as a fluorescent indicator to compare the tumor penetration of POx NPs. As shown in Fig. 5C, the strongest red fluorescence from DiD was observed in tumor slides obtained from DiD/POxA@U treated mice in comparison to that of DiD/PMBEOx treated mice, which also demonstrated POxA@U owned much

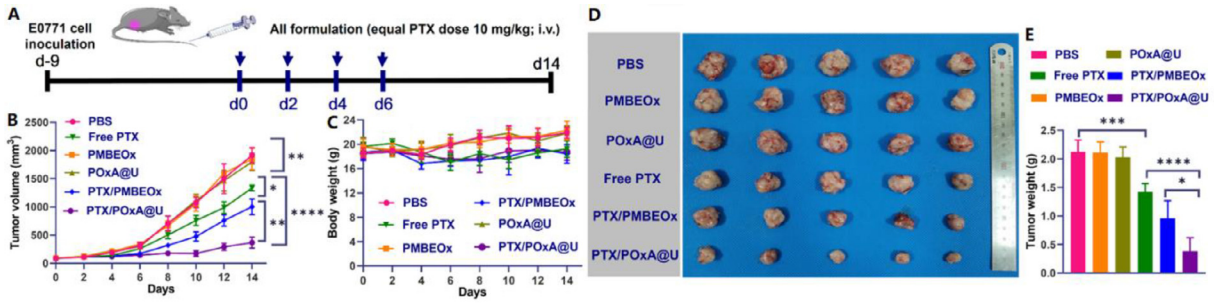

Fig. 6 – Therapeutic results of various PTX formulations in E0771 tumor model. (A) Treatment schedule of the anti-tumor efficacy study. (B) E0771 Tumor volume and (C) changes of body weight of tumor-bearing mice. (D) Photo of excised tumors at day 14. (E) Tumor weight after receiving different treatments; $n = 5$. Results are exhibited as averages ± SD; * $p < 0.05$, ** $p < 0.01$, ***$p < 0.001$, ****P < 0.001.

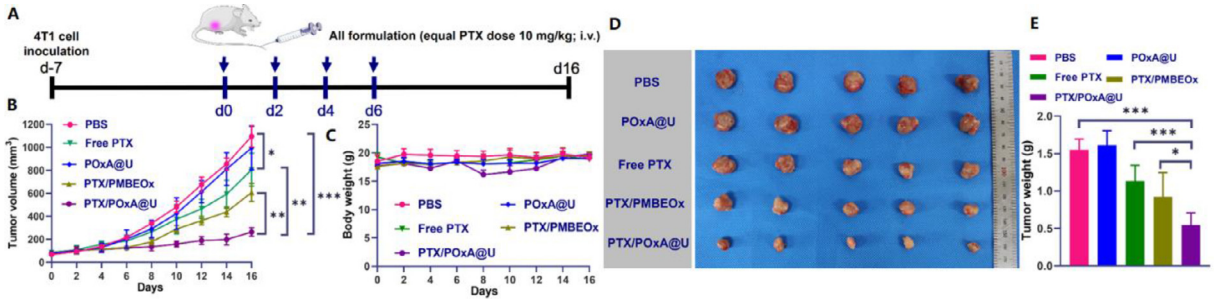

Fig. 7 – Therapeutic results of various PTX formulations in 4T1 tumor model. (A) Treatment schedule of the anti-tumor efficacy study. (B) 4T1 tumor volume and (C) changes of body weight of tumor-bearing mice. (D) Photo of excised tumors at day 16. (e) Tumor weight after recept of different treatments; $n = 5$. Results are exhibited as averages ± SD; * P < 0.05, ** P < 0.01, *** P < 0.001.

stronger tumor accumulation ability compared with DiD/PMBEOx. More importantly, DiD/POxA@U was observed not only around the blood vessels (green fluorescence), but distributed throughout the tumor tissues. However, the DiD fluorescence of DiD/PMBEOx was almost confined near the blood vessels, which could be attributed to that DiD/PMBEOx with a smaller size was much easier to penetrate deeply into tumor tissue [45]. The quantitative analysis of DiD positive areas in the immunofluorescence images is further confirmed that DiD/POxA@U could penetrate much deeper than DiD/PMBEOx (Fig. 5D).

3.5. *In vivo antitumor efficacy*

The *in vivo* anti-tumor efficacy of PTX-loaded NPs were tested on murine breast cancer E0771 model established on C57BL/6 mice. When the tumors were approximately 70 mm^3, mice received the treatments of PBS, free PTX, PMBEOx, POxA@U, PTX/PMBEOx, or PTX/POxA@U every other day for four times on Day 0, 2, 4 and 6. Each injected PTX dose was 10 mg/kg on PTX basis (Fig. 6A). The size of tumors in the PBS, PMBEOx, and POxA@U treated group grew rapidly and was approximately 2000 mm^3 on Day 14. Free PTX treatment also didn't exhibit too much ability for tumor inhibitions at the end of the experiment (Day 14, TSR% = 33.2%). The treatment of PTX/PMBEOx presented moderate therapeutic effect (TSR% = 50.0%). In contrast, the PTX/POxA@U treatment showed the strongest tumor inhibition effect (TSR% = 84.6%) (Fig. 6B, 6D and 6E). Body weight changes of treated mice were monitored throughout the experiment and employed as an indication of antitumor treatment adverse effects. As described in Fig. 6C, no obvious body weight alteration throughout the experiment. The main organs were also stained with hematoxylin and eosin (H&E) for evaluating the safety of the therapeutic treatments. The main organs of experimental groups exhibited typical histomorphology and no significant pathological abnormality was observed, implying no systemic toxicity during the experimental treatment (Fig. S7). The results imply a promoted therapeutic effect for cross-linked NPs in comparison to free PTX in mice. This possibly results from the stable cross-linked core provided a longer blood circulation and more accumulation of PTX in tumor tissues through the EPR effect.

Although PTX/POxA@U NPs showed the most effective antitumor activity in an E0771 tumor-bearing mouse model. We further evaluated the tumor inhibition effect in another murine breast cancer 4T1 model. Similar to the treatment schedule in E0771 model, the 4T1 tumor-bearing mice were intravenously injected 4 times with PBS, free PTX, POxA@U, PTX/PMBEOx, or PTX/POxA@U on Day 0, 2, 4 and 6 (Fig. 7A). As shown in Fig. 7B, 7D and 7E, the PTX-loaded NPs displayed

obvious tumor inhibition *in vivo* compared to the PBS and POxA@U group. Similar to the previous result, compared with free PTX (TSR% = 37.5%) and PTX/PMBEOx (TSR% = 54.2%), the PTX/POxA@U showed the best tumor inhibition effect (TSR% = 70.8%) in the whole treatment in comparison with other groups. Besides, there was no obvious body weight loss (Fig. 7C) and pathological abnormality (Fig. S8) during the treatments. Therefore, the PTX/POxA@U NPs showed great potential in murine breast cancer chemotherapy and other solid tumors.

4. Conclusion

In this study, we prepared a complementary nucleobase core-crosslinked POx NPs for PTX delivery in the treatment of two kinds of breast cancer. The hydrogen bonds between nucleobases A and U in the NPs significantly enhanced the stability of NPs and DLC of PTX (38.3 wt%). These core-crosslinked NPs with smaller sizes showed a promoted accumulation of PTX inside the tumor tissues (8.9 times over free PTX after 24 h). *In vivo* anti-tumor investigations presented that the PTX-loaded core-crosslinked NPs markedly inhibited murine E0771 and 4T1 tumor growth in comparison with free PTX or uncross-linked POx NPs. Moreover, this investigation presented an innovative strategy for fabricating core-crosslinked drug delivery systems that might help treat more kinds of diseases beyond breast cancer and hence would be an attractive platform technique.

Conflicts of interest

The authors report no conflicts of interest. The authors alone are responsible for the content and writing of this article.

Acknowledgements

This work was financially supported by the National Natural Science Foundation of China (51973215, 52025035, 52103194, 22105199, 51829302), Bureau of International Cooperation Chinese Academy of Science (121522KYSB20200029), the Youth Innovation Promotion Association of Chinese Academy of Sciences (2020232).

Supplementary materials

Supplementary material associated with this article can be found, in the online version, at doi:10.1016/j.ajps.2022.04.006.

REFERENCES

[1] Davis ME, Chen Z, Shin DM. Nanoparticle therapeutics: an emerging treatment modality for cancer. Nat Rev Drug Discovery 2008;7:771–82.
[2] Bae YH, Park K. Targeted drug delivery to tumors: myths, reality and possibility. J Control Release 2011;153:198–205.
[3] Zhang XQ, Xu X, Bertrand N, Pridgen E, Swami A, Farokhzad OC. Interactions of nanomaterials and biological systems: implications to personalized nanomedicine. Adv Drug Deliv Rev 2012;64:1363–84.
[4] Ma S, Song W, Xu Y, Si X, Lv S, Zhang Y, et al. Rationally designed polymer conjugate for tumor-specific amplification of oxidative stress and boosting antitumor immunity. Nano Lett 2020;20:2514–21.
[5] Ma S, Song W, Xu Y, Si X, Zhang Y, Tang Z, et al. A ROS-responsive aspirin polymeric prodrug for modulation of tumor microenvironment and cancer immunotherapy. CCS Chemistry 2020;2:390–400.
[6] Lim WT, Tan EH, Toh CK, Hee SW, Leong SS, Ang PCS, et al. Phase I pharmacokinetic study of a weekly liposomal paclitaxel formulation (Genexol-PM) in patients with solid tumors. Ann Oncol 2010;21:382–8.
[7] Chiang NJ, Chang JY, Shan YS, Chen LT. Development of nanoliposomal irinotecan (nal-IRI, MM-398, PEP02) in the management of metastatic pancreatic cancer. Expert Opin Pharmacother 2016;17:1413–20.
[8] Savic R, Luo LB, Eisenberg A, Maysinger D. Micellar nanocontainers distribute to defined cytoplasmic organelles. Science 2003;300:615–18.
[9] Matsumoto Y, Nichols JW, Toh K, Nomoto T, Cabral H, Miura Y, et al. Vascular bursts enhance permeability of tumour blood vessels and improve nanoparticle delivery. Nat Nanotechnol 2016;11:533–8.
[10] Maeda H. Polymer therapeutics and the EPR effect. J Drug Target 2017;25:781–5.
[11] Fang J, Nakamura H, Maeda H. The EPR effect: unique features of tumor blood vessels for drug delivery, factors involved, and limitations and augmentation of the effect. Adv Drug Deliv Rev 2011;63:136–51.
[12] Lv S, Tang Z, Song W, Zhang D, Li M, Liu H, et al. Inhibiting solid tumor growth *in vivo* by non-tumor-penetrating nanomedicine. Small 2017;13.
[13] Wilhelm S, Tavares AJ, Dai Q, Ohta S, Audet J, Dvorak HF, et al. Analysis of nanoparticle delivery to tumours. Nat Rev Mater 2016;1.
[14] Sun X, Wang G, Zhang H, Hu S, Liu X, Tang J, et al. The blood clearance kinetics and pathway of polymeric micelles in cancer drug delivery. ACS Nano 2018;12:6179–92.
[15] Chen H, Kim S, He W, Wang H, Low PS, Park K, et al. Fast release of lipophilic agents from circulating PEG-PDLLA micelles revealed by *in vivo* Forster resonance energy transfer imaging. Langmuir 2008;24:5213–17.
[16] Zhai SD, Hu XL, Hu YJ, Wu BY, Xing D. Visible light-induced crosslinking and physiological stabilization of diselenide-rich nanoparticles for redox-responsive drug release and combination chemotherapy. Biomaterials 2017;121:41–54.
[17] Zhou Z, Li L, Yang Y, Xu X, Huang Y. Tumor targeting by pH-sensitive, biodegradable, cross-linked N-(2-hydroxypropyl) methacrylamide copolymer micelles. Biomaterials 2014;35:6622–35.
[18] Sedlacek O, Monnery BD, Filippov SK, Hoogenboom R, Hruby M. Poly(2-oxazoline)s–are they more advantageous for biomedical applications than other polymers? Macromol Rapid Commun 2012;33:1648–62.
[19] Zalipsky S, Hansen CB, Oaks JM, Allen TM. Evaluation of blood clearance rates and biodistribution of poly(2-oxazoline)-grafted liposomes. J Pharm Sci 1996;85:133–7.
[20] Woodle MC, Engbers CM, Zalipsky S. New amphipatic polymer lipid conjugates forming long-circulating

reticuloendothelial systerm-evading liposomes. Bioconjug Chem 1994;5:493–6.
[21] Konradi R, Pidhatika B, Muehlebach A, Textort M. Poly-2-methyl-2-oxazoline: a peptide-like polymer for protein-repellent surfaces. Langmuir 2008;24:613–16.
[22] Gaertner FC, Luxenhofer R, Blechert B, Jordan R, Essler M. Synthesis, biodistribution and excretion of radiolabeled poly(2-alkyl-2-oxazoline)s. J Control Release 2007;119:291–300.
[23] Somdeb J, Mariusz U. Poly(2-oxazoline)-based stimulus-responsive (Co)polymers: an overview of their design, solution properties, surface-chemistries and applications. Prog Polym Sci 2020.
[24] Han YC, He ZJ, Schulz A, Bronich TK, Jordan R, Luxenhofer R, et al. Synergistic combinations of multiple chemotherapeutic agents in high capacity poly(2-oxazoline) micelles. Mol Pharm 2012;9:2302–13.
[25] Luxenhofer R, Schulz A, Roques C, Li S, Bronich TK, Batrakova EV, et al. Doubly amphiphilic poly(2-oxazoline)s as high-capacity delivery systems for hydrophobic drugs. Biomaterials 2010;31:4972–9.
[26] Hwang D, Ramsey JD, Makita N, Sachse C, Jordan R, Sokolsky-Papkov M, et al. Novel poly(2-oxazoline) block copolymer with aromatic heterocyclic side chains as a drug delivery platform. J Controlled Release 2019;307:261–71.
[27] He ZJ, Wan XM, Schulz A, Bludau H, Dobrovolskaia MA, Stern ST, et al. A high capacity polymeric micelle of paclitaxel: implication of high dose drug therapy to safety and *in vivo* anti-cancer activity. Biomaterials 2016;101:296–309.
[28] Kuang HH, Wu SH, Meng FB, Xie ZG, Jing XB, Huang YB. Core-crosslinked amphiphilic biodegradable copolymer based on the complementary multiple hydrogen bonds of nucleobases: synthesis, self-assembly and *in vitro* drug delivery. J Mater Chem 2012;22:24832–40.
[29] Wang DL, Su Y, Jin CY, Zhu BS, Pang Y, Zhu LJ, et al. Supramolecular copolymer micelles based on the complementary multiple hydrogen bonds of nucleobases for drug delivery. Biomacromolecules 2011;12:1370–9.
[30] Dong S, Ma S, Liu ZL, Ma LL, Zhang Y, Tang ZH, et al. Functional amphiphilic poly(2-oxazoline) block copolymers as drug carriers: the relationship between structure and drug loading capacity. Chin J Polym Sci 2021;39:865–73.
[31] Li S, Feng X, Wang J, Xu W, Islam MA, Sun T, et al. Multiantigenic nanoformulations activate anticancer immunity depending on size. Adv Funct Mater 2019;29.
[32] Song W, Tang Z, Li M, Lv S, Yu H, Ma L, et al. Tunable pH-sensitive poly(beta-amino ester)s synthesized from primary amines and diacrylates for intracellular drug delivery. Macromol Biosci 2012;12:1375–83.
[33] Ma S, Song W, Xu Y, Si X, Zhang D, Lv S, et al. Neutralizing tumor-promoting inflammation with polypeptide-dexamethasone conjugate for microenvironment modulation and colorectal cancer therapy. Biomaterials 2020;232:119676.
[34] Wang YL, Yu HY, Zhang DW, Wang GY, Song WT, Liu YM, et al. Co-administration of combretastatin A4 nanoparticles and sorafenib for systemic therapy of hepatocellular carcinoma. Acta Biomater 2019;92:229–40.
[35] Bouten PJM, Lava K, van Hest JCM, Hoogenboom R. Thermal properties of methyl ester-containing poly(2-oxazoline)s. Polymers (Basel) 2015;7:1998–2008.
[36] Kuang H, Wu S, Meng F, Xie Z, Jing X, Huang Y. Core-crosslinked amphiphilic biodegradable copolymer based on the complementary multiple hydrogen bonds of nucleobases: synthesis, self-assembly and *in vitro* drug delivery. J Mater Chem 2012;22.
[37] Lin IH, Cheng CC, Yen YC, Chang FC. Synthesis and assembly behavior of heteronucleobase-functionalized poly(epsilon-caprolactone). Macromolecules 2010;43:1245–52.
[38] Desai NP, Trieu V, Hwang LY, Wu R, Soon-Shiong P, Gradishar WJ. Improved effectiveness of nanoparticle albumin-bound (nab) paclitaxel *versus* polysorbate-based docetaxel in multiple xenografts as a function of HER2 and SPARC status. Anticancer Drugs 2008;19:899–909.
[39] Kim TY, Kim DW, Chung JY, Shin SG, Kim SC, Heo DS, et al. Phase I and pharmacokinetic study of Genexol-PM, a cremophor-free, polymeric micelle-formulated paclitaxel, in patients with advanced malignancies. Clin Cancer Res 2004;10:3708–16.
[40] Negishi T, Koizumi F, Uchino H, Kuroda J, Kawaguchi T, Naito S, et al. NK105, a paclitaxel-incorporating micellar nanoparticle, is a more potent radiosensitising agent compared to free paclitaxel. Br J Cancer 2006;95:601–6.
[41] Shuai XT, Merdan T, Schaper AK, Xi F, Kissel T. Core-cross-linked polymeric micelles as paclitaxel carriers. Bioconjug Chem 2004;15:441–8.
[42] Sykes EA, Chen J, Zheng G, Chan WCW. Investigating the impact of nanoparticle size on active and passive tumor targeting efficiency. ACS Nano 2014;8:5696–706.
[43] Wang D, Su Y, Jin C, Zhu B, Pang Y, Zhu L, et al. Supramolecular copolymer micelles based on the complementary multiple hydrogen bonds of nucleobases for drug delivery. Biomacromolecules 2011;12:1370–9.
[44] Du JZ, Du XJ, Mao CQ, Wang J. Tailor-made dual pH-sensitive polymer-doxorubicin nanoparticles for efficient anticancer drug delivery. J Am Chem Soc 2011;133:17560–3.
[45] Chen JJ, Ding JX, Wang YC, Cheng JJ, Ji SX, Zhuang XL, et al. Sequentially responsive shell-stacked nanoparticles for deep penetration into solid tumors. Adv Mater 2017;29.